Small-Animal PET Study of Adenosine A_1 Receptors in Rat Brain: Blocking Receptors and Raising Extracellular Adenosine

Soumen Paul[1], Shivashankar Khanapur[1], Anna A. Rybczynska[1], Chantal Kwizera[1], Jurgen W.A. Sijbesma[1], Kiichi Ishiwata[2], Antoon T.M. Willemsen[1], Philip H. Elsinga[1,3], Rudi A.J.O. Dierckx[1,3], and Aren van Waarde[1]

[1]Nuclear Medicine and Molecular Imaging, University Medical Center Groningen, University of Groningen, Groningen, The Netherlands; [2]Positron Medical Center, Tokyo Metropolitan Institute of Gerontology, Tokyo, Japan; and [3]Department of Nuclear Medicine, University Hospital Ghent, Ghent, Belgium

Activation of adenosine A_1 receptors (A_1R) in the brain causes sedation, reduces anxiety, inhibits seizures, and promotes neuroprotection. Cerebral A_1R can be visualized using 8-dicyclopropylmethyl-1-^{11}C-methyl-3-propyl-xanthine (^{11}C-MPDX) and PET. This study aims to test whether ^{11}C-MPDX can be used for quantitative studies of cerebral A_1R in rodents. **Methods:** ^{11}C-MPDX was injected (intravenously) into isoflurane-anesthetized male Wistar rats (300 g). A dynamic scan of the central nervous system was obtained, using a small-animal PET camera. A cannula in a femoral artery was used for blood sampling. Three groups of animals were studied: group 1, controls (saline-treated); group 2, animals pretreated with the A_1R antagonist 8-cyclopentyl-1, 3-dipropylxanthine (DPCPX, 1 mg, intraperitoneally); and group 3, animals pretreated (intraperitoneally) with a 20% solution of ethanol in saline (2 mL) plus the adenosine kinase inhibitor 4-amino-5-(3-bromophenyl)-7-(6-morpholino-pyridin-3-yl)pyrido [2,3-d] pyrimidine dihydrochloride (ABT-702) (1 mg). DPCPX is known to occupy cerebral A_1R, whereas ethanol and ABT-702 increase extracellular adenosine. **Results:** In groups 1 and 3, the brain was clearly visualized. High uptake of ^{11}C-MPDX was noted in striatum, hippocampus, and cerebellum. In group 2, tracer uptake was strongly suppressed and regional differences were abolished. The treatment of group 3 resulted in an unexpected 40%–45% increase of the cerebral uptake of radioactivity as indicated by increases of PET standardized uptake value, distribution volume from Logan plot, nondisplaceable binding potential from 2-tissue-compartment model fit, and standardized uptake value from a biodistribution study performed after the PET scan. The partition coefficient of the tracer (K_1/k_2 from the model fit) was not altered under the study conditions. **Conclusion:** ^{11}C-MPDX shows a regional distribution in rat brain consistent with binding to A_1R. Tracer binding is blocked by the selective A_1R antagonist DPCPX. Pretreatment of animals with ethanol and adenosine kinase inhibitor increases ^{11}C-MPDX uptake. This increase may reflect an increased availability of A_1R after acute exposure to ethanol.

Key Words: receptors; adenosine A1; adenosine kinase inhibitor; brain; positron emission tomography (PET); ethanol

J Nucl Med 2011; 52:1293–1300
DOI: 10.2967/jnumed.111.088005

The adenosine receptor (R) family consists of the A_1, A_{2A}, A_{2B}, and A_3 subtypes. A_1 and A_3R inhibit, whereas A_{2A} and A_{2B} stimulate, production of the second messenger, 3′,5′-cyclic adenosine monophosphate. A_1R and $A_{2A}R$ are activated by nanomolar concentrations of adenosine, whereas A_{2B} and A_3R become activated only when adenosine levels rise into the micromolar range because of inflammation, hypoxia, or ischemia (*1–3*).

A_1Rs are highly expressed and extensively distributed in various regions of the human brain such as the hippocampus, cerebral cortex, thalamic nuclei, and basal ganglia (*4,5*). In the central nervous system, adenosine acts as an endogenous modulator of neurotransmission (*6*), a neuroprotectant (*7*), and an anticonvulsant (*8*). Its neuroprotective action is mediated via A_1R and may be associated with inhibition of the release of excitatory neurotransmitters, hyperpolarization of neurons, and inhibition of Ca^{2+} channels (*9*). Adenosine acts also as an analgesic, by affecting nociceptive afferent and transmission neurons via A_1R (*10*). A_1R agonists usually stimulate (*11*), whereas A_1R antagonists diminish, sleep (*12*). Thus, such compounds may be therapeutically useful. Yet, A_1R agonists have failed to undergo successful clinical development because of dose-limiting cardiovascular side effects.

Adenosine kinase inhibitors (AKIs) represent an alternative treatment strategy. Adenosine kinase (AK) catalyzes a phosphorylation reaction, converting adenosine to adenosine monophosphate (*13,14*). The inhibition of AK decreases the cellular reuptake of adenosine, resulting in increased local adenosine concentrations (*14*). The feasibility of raising adenosine availability in the central nervous system by inhibiting AK has been demonstrated in hippocampal and spinal cord slices (*15*) and by in vivo studies on extracel-

Received Jan. 17, 2011; revision accepted Apr. 11, 2011.
For correspondence or reprints contact: Aren van Waarde, Nuclear Medicine and Molecular Imaging, University Medical Center Groningen, University of Groningen, Hanzeplein 1, 9713 GZ Groningen, The Netherlands.
E-mail: a.van.waarde@ngmb.umcg.nl

lular adenosine in rat striatum, which was increased up to 10-fold (*16*).

The psychoactive drug ethanol also raises extracellular levels of adenosine in the brain (up to 4-fold (*17*)) by augmenting the rate of adenosine formation (*18*) and inhibiting adenosine uptake via nucleoside transporters (*18–20*). The anxiolytic, sedating, and motor-impairing effects of ethanol are related to its interaction with adenosinergic signaling.

PET with a radiolabeled A_1R ligand may allow study of the involvement of A_1R in the pathophysiology of disease, the response of the A_1R population to therapy, and assessment of the occupancy of A_1R by therapeutic drugs. Several positron-emitting A_1R ligands have been prepared for this purpose, but only 2 have been widely used: 8-dicyclopropylmethyl-1-^{11}C-methyl-3-propylxanthine (^{11}C-MPDX) (*21*) and ^{18}F-8-cyclopentyl-3-(3-fluoropropyl)-1-propylxanthine (*5*). Both ligands bind with high affinity and selectivity to A_1R in vivo (K_i and K_d values, 3.0 and 4.4 nM, respectively).

Because small-animal PET studies with ^{11}C-MPDX had not been performed previously, we tested this ligand for quantitative small-animal PET studies in rodents with the intention of later using this technique for the assessment of changes of A_1R density in rodent models of human disease. In addition, we examined the impact of raised levels of extracellular adenosine on the cerebral binding of ^{11}C-MPDX.

MATERIALS AND METHODS

Chemicals

Ethanol and triethylamine were purchased from Merck. The adenosine A_1 antagonist 1,3-dipropyl-8-cyclopentylxanthine (DPCPX) was a product of Sigma, and the potent nonnucleoside 4-amino-5-(3-bromophenyl)-7-(6-morpholino-pyridin-3-yl)pyrido [2,3-d]pyrimidine dihydrochloride (ABT-702) was obtained from Tocris. Stock solutions of DPCPX and ABT-702 were prepared in dimethyl sulfoxide. The radioligand ^{11}C-MPDX was prepared by reaction of ^{11}C-methyl iodide with the appropriate 1-*N*-desmethyl precursor. Briefly, ^{11}C-methyl iodide was trapped in 0.3 mL of *N,N*-dimethylformamide containing 1 mg of 1-*N*-desmethyl precursor and 5 μL of NaOH and was heated at 120°C for 5 min. After 1.0 mL of 0.1 M HCl had been added, the solution was loaded onto a high-performance liquid chromatography column (Econosphere, C_{18}, 5 μm [Altech]; 10 × 250 mm) and eluted with a mixture of 0.1 M NaH_2PO_4 and ethanol (70/30) at a flow rate of 4 mL/min. The fractions containing ^{11}C-MPDX were collected. Retention time of ^{11}C-MPDX was 14 min. The decay-corrected radiochemical yield was 35% ± 5% (based on ^{11}C-methyl iodide), the specific radioactivity was greater than 11 TBq/mmol at the moment of injection, and the radiochemical purity was greater than 98%.

Animal Model

The animal experiments were performed by licensed investigators in compliance with the Law on Animal Experiments of The Netherlands. The protocol was approved by the Committee on Animal Ethics of the University of Groningen. Male Wistar rats were maintained at a 12-h light/12-h dark regime and were fed standard laboratory chow ad libitum (body weights are provided in Table 1).

Small-Animal PET Scanning

In most experiments, 2 rats were scanned simultaneously, using a Focus 220 microPET camera (Siemens-Concorde). Animals were anesthetized with a mixture of isoflurane/air (inhalation anesthesia, 5% ratio during induction, later reduced to <2%). A cannula was placed in a femoral artery for blood sampling. Rats were under anesthesia for 30–40 min before tracer injection (time required for cannulation and transmission scan). The tracer (^{11}C-MPDX) was injected through the penile vein (injected dose is given in Table 1). A list-mode protocol was used (76 min, brain in the field of view). Scanning was started during injection of radioactivity in the lower rat; the upper animal was injected 16 min later. The animal that was injected last was also anesthetized at a later moment. Thus, the duration of anesthesia was similar in all study groups. A series of blood samples (14 samples; volume, 0.10–0.15 mL) was drawn, initially in rapid succession (every 15 s) and later at longer intervals (≤30 min). Plasma was acquired from these samples by short centrifugation (Eppendorf centrifuge, 5 min at 13,000 rpm). Radioactivity in 25 μL of plasma was counted and used as an arterial input function.

For examination of the specificity of tracer binding, 5 animals were pretreated by intraperitoneal injection of DPCPX (1 mg, in 0.3 mL of dimethyl sulfoxide, 15–20 min before injection of the tracer). For examination of the impact of raised levels of extracellular adenosine on ^{11}C-MPDX binding, 5 other rats received ethanol (2 mL of a 20% solution in saline intraperitoneally) and the AKI ABT-702 (1 mg, in 0.3 mL of dimethyl sulfoxide intraperitoneally). Both ethanol and ABT-702 were administered 15–20 min before injection of ^{11}C-MPDX. Control animals (n = 5) received saline only. The ethanol dose that we administered corresponds to substantial consumption of alcohol in humans (about six 0.33-L bottles of normal beer containing 5% alcohol).

List-mode data were reframed into a dynamic sequence of 8 × 30, 3 × 60, 2 × 120, 2 × 180, 3 × 300, 1 × 480, 2 × 600, and 1 × 960 s frames. The data were reconstructed per time frame using an iterative reconstruction algorithm (attenuation-weighted 2-dimensional

TABLE 1
Animal Data

Group	Body weight (g)	Injection in...		ROI size (cm^3)
		MBq	nmol	
Control (n = 5)	299 ± 8	24 ± 10	2.2 ± 0.9	1.02 ± 0.02
DPCPX (n = 5)	314 ± 18	26 ± 14	2.4 ± 1.3	1.02 ± 0.04
Ethanol and ABT-702 (n = 5)	302 ± 16	34 ± 11	3.1 ± 1.0	1.02 ± 0.03
Metabolite analysis (n = 6)	314 ± 14	20 ± 12	1.8 ± 1.1	—

Data are mean ± SD.

ordered-subset expectation maximization, provided by Siemens; 4 iterations, 16 subsets; zoom factor, 2). The final datasets consisted of 95 slices, with a slice thickness of 0.8 mm and an in-plane image matrix of 128 × 128 pixels of size 1 × 1 mm. Datasets were fully corrected for random coincidences, scatter, and attenuation. A separate transmission scan (duration, 515 s) was acquired for attenuation correction. That scan was made before the emission scan. Images were smoothed with a gaussian filter (1.35 mm in both directions).

Small-Animal PET Data Analysis

Three-dimensional regions of interest (ROIs) were manually drawn around the entire brain. Time–activity curves and volumes (cm^3) for the ROIs were calculated, using standard software (Asi-Pro, version 6.2.5.0; Siemens-Concorde). PET standardized uptake values (SUVs) for brain radioactivity were calculated, using measured body weights and injected doses and assuming a specific gravity of 1 g/mL for brain tissue and blood plasma.

Dynamic PET data were analyzed using plasma radioactivity from arterial blood samples as an input function and a graphical method according to Logan (*22*). Because ^{11}C-MPDX proved to be rapidly cleared but slowly metabolized, no metabolite correction of the input function was performed. The error introduced by this procedure (overestimation of the true plasma input) is 10.0% and identical in all study groups; thus, we concluded that metabolite correction could be omitted. Software routines for MatLab 7 (The MathWorks), written by Dr. Antoon T.M. Willemsen (University Medical Center Groningen), were used for curve fitting. The Logan fit was started at 10 min. The cerebral distribution volume (V_T) of the tracer was estimated from the Logan plot. The dynamic PET data were also analyzed using the same input function and software routines, a 2-tissue-compartment model (2TCM), and a fixed blood volume of 3.6%. The partition coefficient (K_1/k_2) and nondisplaceable binding potential (BP_{ND}) (k_3/k_4) of ^{11}C-MPDX were estimated from the model fit. Similar methods were used previously by Kimura et al. (*23*) for quantification of A_1R in the human brain. However, A_1Rs are significantly expressed in rat cerebellum, in contrast to human cerebellum, in which A_1R density is negligible. Therefore, the cerebellum cannot be used as a reference region in small-animal PET studies of the rodent brain.

Biodistribution Studies

After the scanning period, the anesthetized animals were sacrificed. Blood was collected, and plasma and a cell fraction were obtained from the blood sample by short centrifugation (5 min at 1,000*g*). Several brain areas and peripheral tissues (Table 2) were excised. All tissue samples were weighed. The radioactivity in tissue samples was measured using a γ-counter, applying a decay correction. The results were expressed as dimensionless SUVs. The parameter SUV is defined as tissue activity concentration (MBq/g) × body weight (g)/injected dose (MBq).

TABLE 2
Biodistribution Data of ^{11}C-MPDX, 80 Minutes After Injection

Tissue	Control animals (n = 5)	DPCPX-pretreated (n = 5)	Difference vs. control	Ethanol and ABT-702–treated (n = 5)	Difference vs. control
Amygdala	0.75 ± 0.09	0.27 ± 0.05	<0.0001	1.12 ± 0.12	<0.0005
Olfactory bulb	0.64 ± 0.18	0.34 ± 0.07	<0.01	0.75 ± 0.27	NS
Cerebellum	1.34 ± 0.29	0.46 ± 0.09	0.0001	2.16 ± 0.42	<0.01
Cingulate	0.88 ± 0.16	0.35 ± 0.08	0.0001	1.13 ± 0.23	0.06
Entorhinal	0.89 ± 0.10	0.37 ± 0.04	<0.0001	1.27 ± 0.25	<0.01
Frontal	0.89 ± 0.20	0.30 ± 0.08	0.0002	1.16 ± 0.26	NS
Hippocampus	1.09 ± 0.14	0.31 ± 0.08	<0.0001	1.47 ± 0.24	0.01
Medulla	0.75 ± 0.18	0.42 ± 0.11	0.01	1.51 ± 0.29	<0.001
Parietal, temporal, and occipital cortex	0.97 ± 0.20	0.34 ± 0.07	0.0001	1.40 ± 0.48	NS
Pons	0.89 ± 0.21	0.44 ± 0.14	<0.01	1.45 ± 0.30	<0.01
Striatum	1.01 ± 0.13	0.31 ± 0.07	<0.0001	1.18 ± 0.31	NS
Bone	0.24 ± 0.04	0.22 ± 0.09	NS	0.24 ± 0.09	NS
Colon	0.83 ± 0.21	0.61 ± 0.19	NS	0.71 ± 0.06	NS
Duodenum	1.12 ± 0.33	0.95 ± 0.57	NS	1.19 ± 0.17	NS
Fat	1.95 ± 1.15	1.52 ± 0.19	NS	1.06 ± 0.24	NS
Heart	0.69 ± 0.14	0.66 ± 0.08	NS	0.85 ± 0.17	NS
Ileum	1.52 ± 0.52	1.19 ± 0.41	NS	1.38 ± 0.43	NS
Kidney	1.09 ± 0.18	1.26 ± 0.07	0.08	1.50 ± 0.50	NS
Liver	2.94 ± 0.40	4.43 ± 1.03	<0.02	3.63 ± 0.68	NS
Lung	0.70 ± 0.09	0.73 ± 0.07	NS	0.88 ± 0.07	<0.01
Muscle	0.40 ± 0.09	0.48 ± 0.07	NS	0.53 ± 0.07	<0.05
Pancreas	0.98 ± 0.18	1.01 ± 0.23	NS	1.48 ± 0.22	<0.005
Plasma	0.77 ± 0.06	0.73 ± 0.13	NS	0.71 ± 0.13	NS
Red cells	0.34 ± 0.04	0.38 ± 0.09	NS	0.44 ± 0.07	<0.02
Spleen	0.95 ± 0.14	0.65 ± 0.06	<0.005	1.06 ± 0.26	NS
Trachea	0.73 ± 0.15	0.81 ± 0.31	NS	0.85 ± 0.23	NS

SUVs (mean ± SD) are listed.
NS = not significant.

Metabolite Analysis

A separate group of animals ($n = 6$) was used for metabolite analysis. In these rats, a small-animal PET scan was obtained and a biodistribution study was performed, but a smaller series of arterial blood samples was drawn (at intervals of 5, 10, 20, 40, and 60 min after tracer injection, volume increasing from 0.3 to 0.7 mL). Plasma was acquired by short centrifugation (Eppendorf centrifuge, 5 min at 13,000 rpm). Protein was removed by mixing plasma with an equivalent volume of 20% trichloroacetic acid in acetonitrile, followed again by short centrifugation. The protein-free supernatant was injected into a high-performance liquid chromatography system (stationary phase, μBondapak, 7.8 × 300 mm [Waters]; mobile phase, 3% triethylamine and phosphate, pH 2.0: acetonitrile, 60:40 v/v, with a flow rate of 2 mL/min). The retention time of authentic ^{11}C-MPDX (and nonradioactive MPDX) was about 11 min. Two radioactive metabolites eluted at shorter retention times (6 and 8 min, respectively). This reversed-phase system is a slightly modified version of a published analytic procedure (*24*). One-milliliter samples of the eluate were collected at 0.5-min intervals. Radioactivity in these samples was determined with a γ-counter and was automatically corrected for decay.

Statistical Tests

Differences between groups were analyzed using 1-way ANOVA. A probability smaller than 0.05 was considered statistically significant.

RESULTS

Small-Animal PET Images

Small-animal PET images acquired after injection of ^{11}C-MPDX are presented in Figure 1. In saline-treated control animals, the brain was clearly visualized. High tracer uptake was observed in the hippocampus, cerebellum, and striatum (left panel) in addition to some areas of the cortex (image not shown). After pretreatment of rats with DPCPX, cerebral uptake of the tracer was strongly reduced, and regional differences in tracer uptake were no longer apparent (middle panel). When animals were pretreated with ethanol and the AKI ABT-702, a global increase of tracer uptake was noted, compared with the control group (right panel).

Kinetics of Radioactivity in Brain and Plasma

Cerebral kinetics of ^{11}C-MPDX–derived radioactivity (PET SUV in the whole brain as a function of time) are presented in Figure 2. In saline-treated control animals, uptake of the tracer rapidly increased to a maximum, which was already reached between 7 and 12 min, and was followed by washout. In animals pretreated with DPCPX, only a rapid washout of tracer was observed, and the cerebral uptake of ^{11}C was strongly reduced. In rats pretreated with ABT-702 and ethanol, cerebral uptake of radioactivity was significantly increased, compared with the control group. Maximal tracer uptake now occurred after 13–20 min and was followed by washout.

On the basis of SUVs measured with small-animal PET, A_1R densities reported in the literature (e.g., 5,003 fmol of protein per milligram in rat hippocampus (*25*)), injected masses of the tracer (Table 1), and assuming that cerebral tissue contains 10% protein, we estimate that less than 5% of the A_1R population in the rat brain was occupied by ^{11}C-MPDX under the conditions of our study.

Kinetics of radioactivity in rat plasma after injection of ^{11}C-MPDX are presented in Figure 2. A rapid, biexponential clearance was observed in all groups. Treatment of animals with DPCPX or a combination of ethanol and AKI (ABT-702) did not significantly affect tracer clearance from the plasma compartment. Areas under the curve (percentage of control) were 100.0 ± 8.4, 95.5 ± 6.6, and 96.0 ± 7.5 for the baseline, ethanol and ABT-702, and DPCPX groups, respectively (mean ± SEM).

Metabolite Analysis

The appearance of radiolabeled metabolites in rat plasma after injection of ^{11}C-MPDX was studied in 2 untreated control animals, 2 rats treated with ethanol and ABT-702, and 2 rats pretreated with DPCPX. Injected ^{11}C-MPDX was found to be hardly metabolized. The fraction of parent compound decreased from almost 100% at time zero to 82%–84% at 60 min (Fig. 3). Pretreatment did not affect the rate of tracer metabolism.

Biodistribution Data

Biodistribution data of ^{11}C, acquired 80 min after injection of ^{11}C-MPDX, are presented in Table 2. Pretreatment of animals with DPCPX resulted in a highly significant reduction of tracer uptake in all studied brain areas. Among peripheral organs, a significant reduction of tracer uptake was observed only in the spleen. DPCPX treatment caused

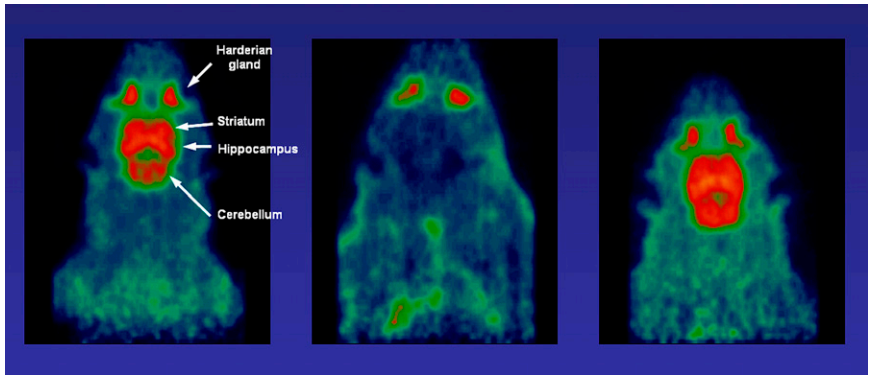

FIGURE 1. Small-animal PET images of rat brain acquired after injection of ^{11}C-MPDX (summed frames from 2 min to end of scan, SUV maximum set to 3): untreated control animal (left), animal pretreated with DPCPX (middle), and animal pretreated with ethanol and ABT-702 (right).

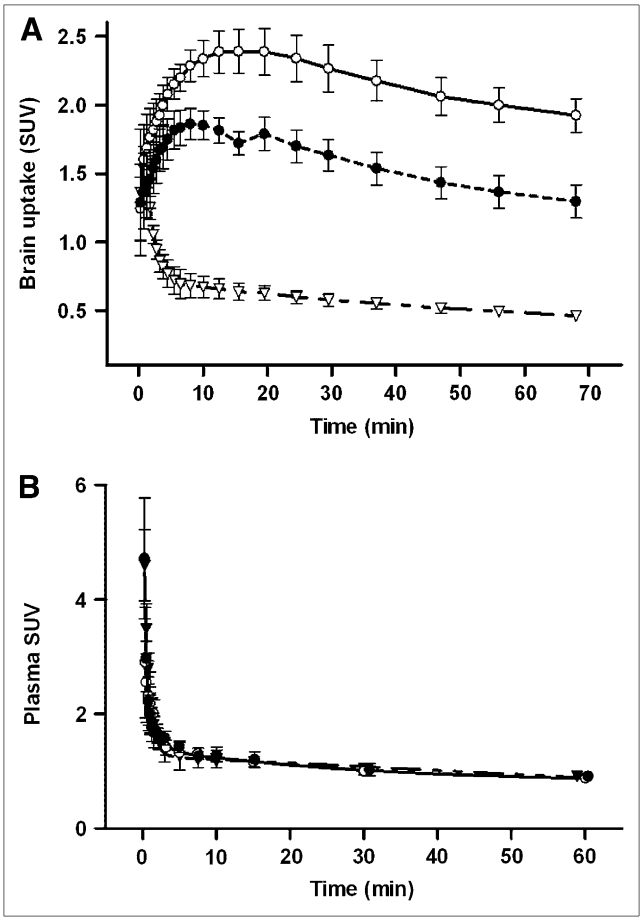

FIGURE 2. Kinetics of ^{11}C-MPDX–derived radioactivity in rat brain (A) and plasma (B). Error bars indicate SEM. Plasma data are not corrected for metabolites. ● = control group; ○ = ethanol and ABT-702–treated animals; ▽ = animals pretreated with DPCPX.

a significant increase of the amount of radioactivity in the liver. Renal uptake of the tracer appeared to be increased as well, but the change was relatively small and this trend did not reach statistical significance.

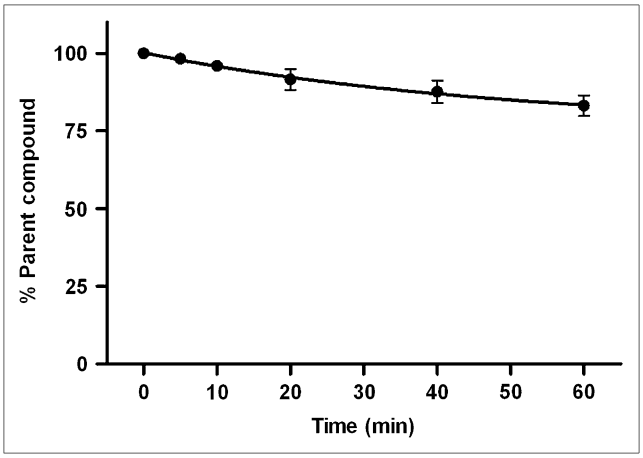

FIGURE 3. Fraction of plasma radioactivity representing parent ^{11}C-MPDX. Pooled data are used because group differences were not observed. Error bars indicate SEM.

Treatment of rats with ethanol and ABT-702 increased uptake of radioactivity in the brain. This increase was statistically significant in the amygdala, cerebellum, entorhinal cortex, hippocampus, medulla, and pons. In other brain areas, an increase was also noted but this trend did not reach statistical significance because of a relatively large individual variance in the study groups. Outside the brain, increases of tracer uptake were noted in lungs, skeletal muscle, pancreas, and red blood cells after treatment of animals with ethanol and ABT-702.

Graphical Analysis of PET Data

V_T of tracer was calculated using a Logan plot (Fig. 4), time–activity curves from an ROI drawn around the entire brain, and radioactivity counts from arterial blood samples. V_T of tracer was significantly decreased (by 63%) after pretreatment of animals with DPCPX and significantly increased (by 39%) after pretreatment with ethanol and ABT-702 (Table 3).

Compartment Modeling of PET Data

A 2TCM was fitted to time–activity curves from an ROI drawn around the entire brain, using radioactivity counts from arterial blood samples as an input function. A 1-tissue-compartment model could not be fitted to the time–activity curves of control and ethanol and ABT-702–treated animals at all, in contrast to a 2TCM. Thus, the 2TCM was clearly superior. The partition coefficient of ^{11}C-MPDX (ratio K_1/k_2 from the model fit) was not significantly affected by any of the treatments, in contrast to BP_{ND} (Table 3). BP_{ND} was reduced to zero after treatment of animals with DPCPX and significantly increased (by 54%) after treatment with ethanol and ABT-702. V_T calculated from the 2TCM fit corresponded closely to V_T acquired by graphical (Logan) analysis of the PET data, although the intraindividual variability was greater. V_T (from the model fit) was significantly reduced (by 63%) after pretreatment of animals with DPCPX and significantly increased (by 42%) after treatment with ethanol and ABT-702.

DISCUSSION

Specificity of ^{11}C-MPDX Binding

The regional distribution of radioactivity in the rat brain after injection of ^{11}C-MPDX (Fig. 1, left) suggests that this tracer is capable of visualizing regional A_1R densities. Further evidence for specific in vivo binding of ^{11}C-MPDX was obtained by pretreating animals with the subtype-selective antagonist DPCPX. In pretreated animals, the brain uptake of radioactivity after injection of ^{11}C-MPDX was strongly suppressed, and regional differences were no longer evident (Fig. 1, middle; Fig. 2, top). A biodistribution study, performed at 80 min after tracer injection, confirmed that uptake of radioactivity was reduced by DPCPX to a low value that was homogeneous throughout the brain (Table 2). The greatest declines were observed in the hippocampus (72%), striatum (69%), cerebellum (66%), frontal cortex (66%), parietal cortex (65%), and amygdala (64%). Outside the brain, a

TABLE 3
Results from Graphical Analysis and Compartment Modeling of PET Data (ROI Drawn Around Entire Brain)

Parameter	V_T (Logan)	K_1/k_2 (2TCM)	BP_{ND} (k_3/k_4) (2TCM)	V_T (2TCM)
Control rats	1.52 ± 0.18	0.62 ± 0.17	1.52 ± 0.10	1.56 ± 0.37
DPCPX-pretreated	0.57 ± 0.05	0.58 ± 0.07	0.00	0.58 ± 0.07
	$P < 0.0001$	P = NS	$P < 0.0001$	$P < 0.0001$
Ethanol and ABT-702–pretreated	2.12 ± 0.25	0.68 ± 0.17	2.34 ± 0.64	2.21 ± 0.44
	$P < 0.005$	P = NS	$P < 0.05$	$P < 0.05$

Mean ± SD P values relate to effect of pretreatment, compared with untreated controls.
NS = not significant.

reduction of ^{11}C-MPDX uptake was observed only in the spleen, possibly reflecting specific binding of the tracer to A_1R, because A_1Rs are involved in splenic contraction (*26*). DPCPX caused a significant increase of the levels of radioactivity in rat liver and tended to increase renal activity levels as well (Table 2), indicating that after blocking of the receptor compartment, a greater fraction of the injected dose is taken up by organs involved in tracer excretion.

To further test the origin of the PET signal, we plotted the specific binding of ^{11}C-MPDX in various brain areas (uptake in saline-treated control animals minus uptake in animals pretreated with DPCPX, Table 2) against regional A_1R numbers, known from autoradiography (*27–29*). The regions plotted were the amygdala, cerebellum, cingulate, entorhinal, and frontal cortices; hippocampus; medulla; parietal–temporal–occipital cortex; pons; and striatum. Receptor density in the hippocampus (main target region) was set to 100%, to allow the use of data from several published studies. An excellent correlation was observed between literature values for A_1R density and ^{11}C-MPDX uptake at 80 min after injection (Fig. 5).

Data analysis of the cerebral time–activity curves in saline- and DPCPX-treated animals also confirmed specific binding of ^{11}C-MPDX to cerebral A_1R. Tracer V_T in the entire brain—calculated either by graphical analysis or by kinetic modeling of the PET data—showed a decline (>60%) similar to that of tracer SUV measured after 80 min (Table 3). In contrast, BP_{ND} of ^{11}C-MPDX estimated by fitting a 2TCM was reduced to zero after pretreatment of animals with DPCPX (Table 3), suggesting that specific binding of ^{11}C-MPDX is absent in DPCPX-treated animals.

Effect of Ethanol and Inhibition of Adenosine Kinase

Acute administration of ethanol is known to result in strong increases of extracellular adenosine both in cell culture and in the rat brain in vivo, which can be assessed by microdialysis (*17*). Two different mechanisms may underlie this effect of ethanol. First, ethanol is metabolized to acetate and acetyl-coA before entering the tricarboxylic acid cycle. Increased flux through acetyl coA-synthetase leads to increased production of adenosine from adenosine monophosphate via 5′-nucleotidase and stimulation of cellular adenosine release (*18*). Second, ethanol blocks nucleoside transporters in cellular membranes, particularly the type 1 equilibrative nucleoside transporter (*19,20,30,31*). Increased binding of adenosine to cerebral A_1R is believed to be an important factor underlying the motor incoordination (*32–35*) and sleep-promoting (*36*) effects of ethanol.

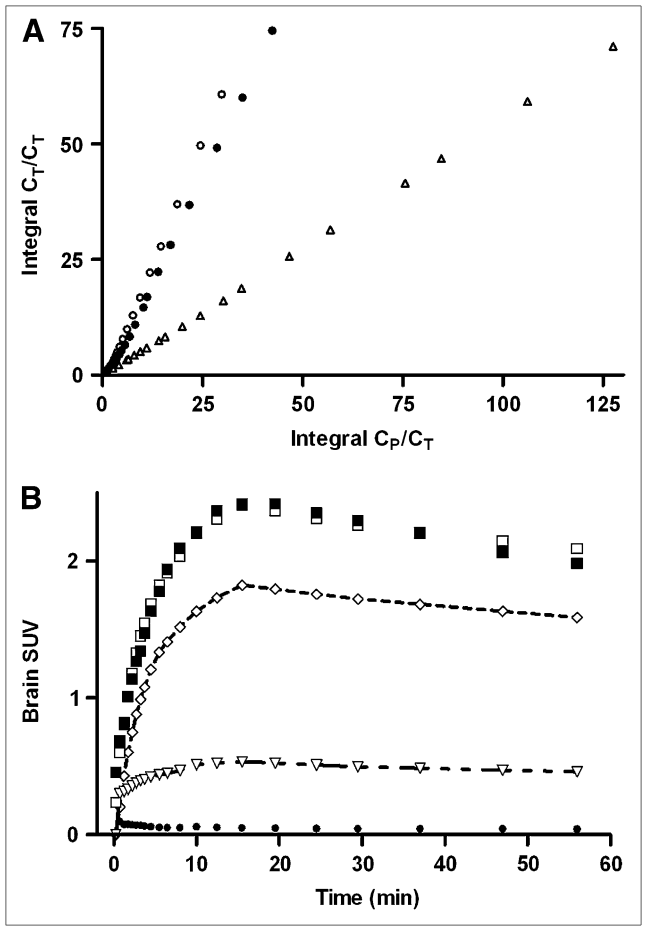

FIGURE 4. Logan plots (A) of control, ethanol and ABT-702–treated, and DPCPX-treated rats and 2TCM fit (B) for animal pretreated with ethanol and ABT-702. (A) ● = control group; ○ = ethanol and ABT-702–treated animals; △ = animals pretreated with DPCPX. (B) ■ = measured activity in brain; □ = fitted activity in brain, ◇ = specific binding in brain; ▽ = nondisplaceable binding in brain and tracer in plasma; ♦ = tracer in plasma.

The coadministration of an AKI (e.g., ABT-702) with ethanol leads to even stronger increases of extracellular adenosine, because phosphorylation of adenosine by the enzyme AK is normally the primary route of adenosine metabolism. Inhibition of AK decreases the rate of adenosine inactivation and locally enhances extracellular adenosine concentrations—not at baseline but rather under conditions of increased formation of adenosine. Orally administered AKIs are known to raise regional concentrations of endogenous adenosine in the brain (*15,16*), and for this reason, these compounds have therapeutic potential as analgesic, antiinflammatory, and antiepileptic agents (*14,37*).

Because both ethanol administration and AK inhibition are known to increase the levels of extracellular adenosine, we expected to observe a decreased binding of the PET tracer ^{11}C-MPDX in the rat brain after acute treatment of rats with ethanol and ABT-702. Competition of adenosine for tracer binding to A_1R is likely to occur, because the affinities of adenosine and ^{11}C-MPDX for cerebral A_1R are in the same (nanomolar) range (*38*). However, in ethanol and ABT-702–pretreated animals, we observed a paradoxic increase rather than a decrease of cerebral tracer binding. Statistically significant increases occurred in PET SUV (Figs. 1 and 2), SUV from an ex vivo biodistribution study (Table 2), and tracer V_T (Table 3).

Kinetic modeling was performed to gain more insight into the mechanisms underlying the paradoxic increase of cerebral radioactivity induced by ethanol and ABT-702. Fitting of a 2TCM to the cerebral time–activity curves of control and treated animals indicated that the partition coefficient of the tracer (K_1/k_2) was not affected by treatment, in contrast to BP_{ND}, which showed a significant increase (Table 3). The fit data, and also our data on tracer clearance (Fig. 2) and metabolism (Fig. 3), suggest that tracer delivery is not changed by treatment. Increases of the apparent A_1R densities (on average, 35%; maximally, 55%) in the brain of rats and mice have been reported, both after acute (*32,39*) and after chronic (*39,40*) administration of ethanol, using ex vivo binding assays. Such changes could cause increased cerebral binding of ^{11}C-MPDX after treatment of rodents with ethanol and ABT-702. However, further studies are necessary to identify the mechanism underlying increased binding of the A_1R ligand under these conditions.

CONCLUSION

Our data suggest that regional A_1R densities in rat brain can be assessed using the tracer ^{11}C-MPDX and small-animal PET. In the brain of untreated control animals, the highest levels of tracer uptake were observed in target regions with a high density of A_1R, such as the hippocampus, striatum, cerebellum, and cerebral cortex (Fig. 1). Pretreatment of animals with the specific A_1R antagonist DPCPX resulted in a strong suppression of tracer uptake in the central nervous system and an abolishment of the regional differences (Fig. 1; Table 2). Specific binding of the tracer in various brain regions corresponded closely to regional A_1R densities known from autoradiography (Fig. 5). Tracer binding can be quantified both by graphical analysis (Logan plot, calculation of V_T) and by kinetic modeling (BP_{ND} or V_T from 2TCM, Table 3). The PET data did not provide evidence for increased competition of endogenous adenosine after acute treatment of animals with ethanol and ABT-702, but a globally increased binding of ^{11}C-MPDX was noted in the rat brain (Figs. 1 and 2; Tables 2 and 3), which may correspond to increases of apparent A_1R density reported in the literature. Further studies are necessary to elucidate the mechanisms underlying the enhanced ^{11}C-MPDX binding after treatment of animals with ethanol and ABT-702.

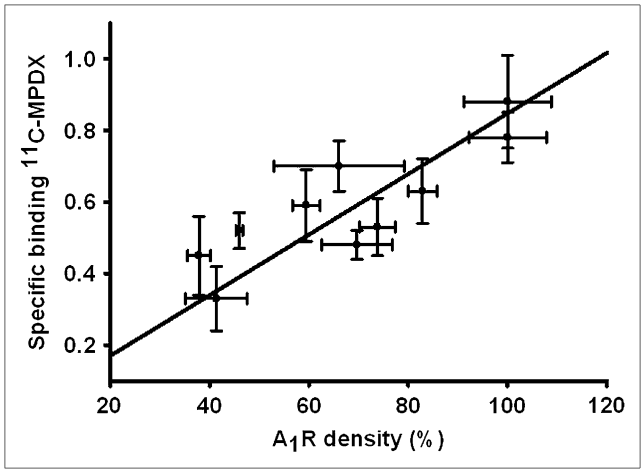

FIGURE 5. Correlation between specific in vivo binding of ^{11}C-MPDX and regional A_1R density as known from autoradiography.

DISCLOSURE STATEMENT

The costs of publication of this article were defrayed in part by the payment of page charges. Therefore, and solely to indicate this fact, this article is hereby marked "advertisement" in accordance with 18 USC section 1734.

ACKNOWLEDGMENT

No potential conflict of interest relevant to this article was reported.

REFERENCES

1. Collis MG, Hourani SM. Adenosine receptor subtypes. *Trends Pharmacol Sci.* 1993;14:360–366.
2. Fredholm BB, Abbracchio MP, Burnstock G, et al. Nomenclature and classification of purinoceptors. *Pharmacol Rev.* 1994;46:143–156.
3. Haas HL, Selbach O. Functions of neuronal adenosine receptors. *Naunyn Schmiedebergs Arch Pharmacol.* 2000;362:375–381.
4. Fastbom J, Pazos A, Probst A, Palacios JM. Adenosine A1 receptors in the human brain: a quantitative autoradiographic study. *Neuroscience.* 1987;22:827–839.
5. Bauer A, Holschbach MH, Meyer PT, et al. In vivo imaging of adenosine A1 receptors in the human brain with [^{18}F]CPFPX and positron emission tomography. *Neuroimage.* 2003;19:1760–1769.
6. Williams M. Adenosine: a selective neuromodulator in the mammalian CNS? *Trends Neurosci.* 1984;7:164–168.
7. Fredholm BB. Adenosine and neuroprotection. *Int Rev Neurobiol.* 1997;40:259–280.
8. Young D, Dragunow M. Status epilepticus may be caused by loss of adenosine anticonvulsant mechanisms. *Neuroscience.* 1994;58:245–261.

9. Dunwiddie TV, Masino SA. The role and regulation of adenosine in the central nervous system. *Annu Rev Neurosci.* 2001;24:31–55.
10. Sawynok J, Reid A, Poon A. Peripheral antinociceptive effect of an adenosine kinase inhibitor, with augmentation by an adenosine deaminase inhibitor, in the rat formalin test. *Pain.* 1998;74:75–81.
11. Portas CM, Thakkar M, Rainnie DG, Greene RW, McCarley RW. Role of adenosine in behavioral state modulation: a microdialysis study in the freely moving cat. *Neuroscience.* 1997;79:225–235.
12. Lin AS, Uhde TW, Slate SO, McCann UD. Effects of intravenous caffeine administered to healthy males during sleep. *Depress Anxiety.* 1997;5:21–28.
13. Arch JR, Newsholme EA. The control of the metabolism and the hormonal role of adenosine. *Essays Biochem.* 1978;14:82–123.
14. McGaraughty S, Cowart M, Jarvis MF. Recent developments in the discovery of novel adenosine kinase inhibitors: mechanism of action and therapeutic potential. *CNS Drug Rev.* 2001;7:415–432.
15. Golembiowska K, White TD, Sawynok J. Adenosine kinase inhibitors augment release of adenosine from spinal cord slices. *Eur J Pharmacol.* 1996;307:157–162.
16. Britton DR, Mikusa J, Lee CH, et al. Site and event specific increase of striatal adenosine release by adenosine kinase inhibition in rats. *Neurosci Lett.* 1999;266:93–96.
17. Sharma R, Engemann SC, Sahota P, Thakkar MM. Effects of ethanol on extracellular levels of adenosine in the basal forebrain: an in vivo microdialysis study in freely behaving rats. *Alcohol Clin Exp Res.* 2010;34:813–818.
18. Nagy LE. Ethanol metabolism and inhibition of nucleoside uptake lead to increased extracellular adenosine in hepatocytes. *Am J Physiol.* 1992;262:C1175–C1180.
19. Nagy LE, Diamond I, Casso DJ, Franklin C, Gordon AS. Ethanol increases extracellular adenosine by inhibiting adenosine uptake via the nucleoside transporter. *J Biol Chem.* 1990;265:1946–1951.
20. Krauss SW, Ghirnikar RB, Diamond I, Gordon AS. Inhibition of adenosine uptake by ethanol is specific for one class of nucleoside transporters. *Mol Pharmacol.* 1993;44:1021–1026.
21. Fukumitsu N, Ishii K, Kimura Y, et al. Imaging of adenosine A1 receptors in the human brain by positron emission tomography with [^{11}C]MPDX. *Ann Nucl Med.* 2003;17:511–515.
22. Logan J. Graphical analysis of PET data applied to reversible and irreversible tracers. *Nucl Med Biol.* 2000;27:661–670.
23. Kimura Y, Ishii K, Fukumitsu N, et al. Quantitative analysis of adenosine A1 receptors in human brain using positron emission tomography and [1-methyl-^{11}C] 8-dicyclopropylmethyl-1-methyl-3-propylxanthine. *Nucl Med Biol.* 2004;31: 975–981.
24. Furuta R, Ishiwata K, Kiyosawa M, et al. Carbon-11-labeled KF15372: a potential central nervous system adenosine A1 receptor ligand. *J Nucl Med.* 1996;37:1203–1207.
25. Elmenhorst D, Basheer R, McCarley RW, Bauer A. Sleep deprivation increases A(1) adenosine receptor density in the rat brain. *Brain Res.* 2009;1258:53–58.
26. Fozard JR, Milavec-Krizman M. Contraction of the rat isolated spleen mediated by adenosine A1 receptor activation. *Br J Pharmacol.* 1993;109:1059–1063.
27. Fastbom J, Pazos A, Palacios JM. The distribution of adenosine A1 receptors and 5′-nucleotidase in the brain of some commonly used experimental animals. *Neuroscience.* 1987;22:813–826.
28. Kanai Y, Araki T, Kato H, Kogure K. Autoradiographic distribution of neurotransmitter and second messenger system receptors in animal brains. *Behav Brain Res.* 1994;65:67–73.
29. Daval JL, Werck MC, Nehlig A, Pereira de Vasconcelos A. Quantitative autoradiographic study of the postnatal development of adenosine A1 receptors and their coupling to G proteins in the rat brain. *Neuroscience.* 1991;40:841–851.
30. Choi DS, Cascini MG, Mailliard W, et al. The type 1 equilibrative nucleoside transporter regulates ethanol intoxication and preference. *Nat Neurosci.* 2004;7:855–861.
31. King AE, Ackley MA, Cass CE, Young JD, Baldwin SA. Nucleoside transporters: from scavengers to novel therapeutic targets. *Trends Pharmacol Sci.* 2006;27:416–425.
32. Clark M, Dar MS. In vitro autoradiographic evidence for adenosine modulation of ethanol-induced motor disturbances in rats. *Alcohol Alcohol Suppl.* 1991;1: 203–206.
33. Phan TA, Gray AM, Nyce JW. Intrastriatal adenosine A1 receptor antisense oligodeoxynucleotide blocks ethanol-induced motor incoordination. *Eur J Pharmacol.* 1997;323:R5–R7.
34. Dar MS, Mustafa SJ. Acute ethanol/cannabinoid-induced ataxia and its antagonism by oral/systemic/intracerebellar A1 adenosine receptor antisense in mice. *Brain Res.* 2002;957:53–60.
35. Connole L, Harkin A, Maginn M. Adenosine A1 receptor blockade mimics caffeine's attenuation of ethanol-induced motor incoordination. *Basic Clin Pharmacol Toxicol.* 2004;95:299–304.
36. Thakkar MM, Engemann SC, Sharma R, Sahota P. Role of wake-promoting basal forebrain and adenosinergic mechanisms in sleep-promoting effects of ethanol. *Alcohol Clin Exp Res.* 2010;34:997–1005.
37. Kowaluk EA, Jarvis MF. Therapeutic potential of adenosine kinase inhibitors. *Expert Opin Investig Drugs.* 2000;9:551–564.
38. Noguchi J, Ishiwata K, Furuta R, et al. Evaluation of carbon-11 labeled KF15372 and its ethyl and methyl derivatives as a potential CNS adenosine A1 receptor ligand. *Nucl Med Biol.* 1997;24:53–59.
39. Jarvis MF, Becker HC. Single and repeated episodes of ethanol withdrawal increase adenosine A1, but not A2A, receptor density in mouse brain. *Brain Res.* 1998;786:80–88.
40. Daly JW, Shi D, Wong V, Nikodijevic O. Chronic effects of ethanol on central adenosine function of mice. *Brain Res.* 1994;650:153–156.